

This is the accepted version of the following article:

Dong, W., Krbal, M., Kalikka, J., Chin, X. Y., Gholipour, B., Soci, C., . . . Simpson, R. E. (2016). Enhanced Sb<sub>2</sub>S<sub>3</sub> crystallisation by electric field induced silver doping. *Thin Solid Films*, 616, 80-85.  
doi:10.1016/j.tsf.2016.07.068

This postprint version is available from URI: <http://hdl.handle.net/10195/67603>

Publisher's version is available from

<http://www.sciencedirect.com/science/article/pii/S0040609016304175?via%3Dihub>



This postprint version is licenced under a [Creative Commons Attribution-NonCommercial-NoDerivatives 4.0 International](https://creativecommons.org/licenses/by-nc-nd/4.0/).

# Enhanced $\text{Sb}_2\text{S}_3$ crystallisation by electric field induced silver doping

Weiling Dong<sup>1</sup>, Milos Krbal<sup>2</sup>, Janne Kalikka<sup>1</sup>, Xin Yu Chin<sup>3</sup>, Behrad Gholipour<sup>3</sup>, Cesare Soci<sup>3</sup>, P. blue J. Fons<sup>4,5</sup>, Kirill V. Mitrofanov<sup>4</sup>, Lujie Chen<sup>1</sup>, Robert E. Simpson<sup>1</sup>

<sup>1</sup>*Singapore University of Technology and Design, 8 Somapah Road, Singapore, 487372*

<sup>2</sup>*Center of Materials and Nanotechnologies (CEMNAT), Faculty of Chemical Technology, University of Pardubice, Legions Square 565, 530 02 Pardubice, Czech Republic*

<sup>3</sup>*Nanyang Technological University, Singapore 637371*

<sup>4</sup>*Nanoelectronics Research Institute, National Institute of Advanced Industrial Science and Technology 1-1-1 Higashi, Tsukuba 305-8565, Ibaraki, Japan*

<sup>5</sup>*SPRING8, Japan Synchrotron Radiation Institute (JASRI), Kouto 1-1-1, Sayo-cho, Sayo-gun, Hyogo 679-5198, Japan*

---

## Abstract

This work reveals that doping Ag into  $\text{Sb}_2\text{S}_3$  substantially decreases its crystallisation temperature. We show that applying an electric field to  $\text{Sb}_2\text{S}_3$  through Ag electrodes provides control of the crystallisation temperature and crystallisation rate. The crystal nuclei incubation time decreases substantially when the applied electric field is set to 200 kV/m. The applied electric field appears to force the Ag cations through the amorphous chalcogenide film resulting in Ag doped  $\text{Sb}_2\text{S}_3$  filaments that extend from the cathode to the anode. This was confirmed by X-ray fluorescence composition mapping. Density functional theory molecular dynamics modelling of Ag doped  $\text{Sb}_2\text{S}_3$  reveals that the diffusion constant of Ag is twice that of Sb or S over a wide temperature range, which implies that the Ag atoms are mobile in the amorphous  $\text{Sb}_2\text{S}_3$  structure. The applied electric field provides a mechanism to enhance the crystallisation kinetics of Ag-doped  $\text{Sb}_2\text{S}_3$ .

**Keywords:**  $\text{Sb}_2\text{S}_3$ , chalcogenide, dissolution, crystallisation

---

*Email address:* weiling\_dong@mymail.sutd.edu.sg (Weiling Dong<sup>1</sup>)

---

## 1. INTRODUCTION

Amorphous  $\text{Sb}_2\text{S}_3$  is a weakly polar semiconducting ferroelectric material with high photosensitivity and thermoelectric power[1, 2], and it crystallises into an orthorhombic layered structure at a temperature that ranges from 526 K to 584 K depending on the size of the particles and the heating conditions[3]. This phase transition predominantly results from small structural changes in the coordination sphere of Sb atoms[4]. The band gap of  $\text{Sb}_2\text{S}_3$  is dependent on the preparation conditions and can vary between 1.8 and 2.5 eV[5, 6], which covers the solar spectrum. Due to the aforementioned special properties,  $\text{Sb}_2\text{S}_3$  has been developed for a multitude of applications, such as lithium ion batteries[7, 8, 9], hydrogen storage[10, 11], catalysts for Dye-Sensitized Solar Cells (DSSC)[12], photodetectors[2] and optical recording media[13].

Silver doped  $\text{Sb}_2\text{S}_3$  exhibits a red-shifted absorption edge and consequently a reduced optical bandgap[14, 15, 16, 17, 18]. Its refractive index has been measured to increase by about 0.2 with silver content up to 8.2 at.% Ag[19]. Therefore, this material is attractive for potential applications in photonics. Generally, silver doped chalcogenides have found various applications in photonics and electronics. For example, silver doping has been successfully used to pattern low loss GeS waveguides using a photo-dissolution process[20]. Two-dimensional anisotropic layered  $\text{Bi}_2\text{Se}_3$  chalcogenide nanoribbons that allow superstoichiometric intercalation of metal atoms such as Ag, Au, Co, Cu, Fe, In, Ni and Sn at the van der Waals gap of the host chalcogenide have also been investigated for potential atomic storage applications[21]. Others explored silver doped  $\text{Ge}_{46}\text{S}_{54}$  thin films for use in potential programmable metallisation cell (PMC) memory devices, where the intrinsic high resistance of the device can be switched to a low resistance state by growing a stable silver electrodeposited link from the cathode to the anode. A reverse bias dissolves the electrodeposit, causing the device resistance to increase[22].

Photo-induced dissolution and diffusion of silver in chalcogenide films is a

30 well known effect. The silver lateral diffusion process has been explained by considering the doped chalcogenide/undoped chalcogenide interface as a p-n junction. The undoped chalcogenide is modelled as p-type material whilst the doped material is n-type. The electric field of the junction pulls the Ag ions into the undoped region. As the lattice undergoes structural rearrangements caused  
35 by the photo excitation of interfacial electrons, mechanical stress is generated at the boundary arising from differences in the lattice parameters of the undoped and doped materials. This stress contributes to large structural rearrangements, including bond breaking induced formation of voids into which the silver ions can easily penetrate[23, p. 165].

40 We use a combination of  $\text{Sb}_2\text{S}_3$  thin films, Ag electrodes and an electric field to enhance the crystal nucleation process in the  $\text{Sb}_2\text{S}_3$  thin films. Ag doping in  $\text{Sb}_2\text{S}_3$  via photo dissolution is a known effect, however, there are no reports about electric field-assisted migration of Ag in  $\text{Sb}_2\text{S}_3$ . Moreover, we are not aware of any reports that suggest using silver electro-doping to enhance  
45 the crystallisation of chalcogenide materials. The objective of this work is to enhance the crystallisation kinetics of  $\text{Sb}_2\text{S}_3$  films through electric field induced Ag doping. The effect of silver doping on the crystallisation of  $\text{Sb}_2\text{S}_3$  is explored. The crystallisation rate, crystal growth direction and the crystallisation kinetics are altered by varying the applied electric field and temperature of the film.

## 50 METHODS

$\text{Sb}_2\text{S}_3$  films were prepared on fused silica substrates by radio frequency sputtering. The chamber base pressure was  $2.6 \times 10^{-5}$  Pa, and the sputtering pressure was 0.5 Pa. The deposition rate was  $0.43 \text{ \AA}/\text{min}$  from an  $\text{Sb}_2\text{S}_3$  alloy target of diameter of 50.8 mm and a purity of 99.9 %. Ag doped films with different silver concentration were prepared by attaching Ag pellets with different  
55 sizes on to the  $\text{Sb}_2\text{S}_3$  target, a doping method used by other researchers[24]. The composition of the films was analysed by energy dispersive x-ray (EDX) spectroscopy in a scanning electron microscope (SEM).

The effect of silver doping on the crystallisation temperature of  $\text{Sb}_2\text{S}_3$  was  
60 studied by measuring the crystal growth of Ag-doped  $\text{Sb}_2\text{S}_3$  samples as a func-  
tion of temperature. A microscope furnace was used to heat the films at  
10 K/min in an Ar atmosphere flowing at a rate of  $10 \text{ cm}^3/\text{min}$ . The over-  
all crystallisation temperature of the films was obtained by monitoring the in-  
tensity of the reflected light as a function of temperature. Crystallisation of  
65  $\text{Sb}_2\text{S}_3$  produces a large reduction in the intensity of the reflected light. The  
maximum rate of change in reflectivity was assumed to occur at the maximum  
crystallisation rate.

The force on charged particles is proportional to the external electric field,  
thus we expect silver cations to be electrically forced into  $\text{Sb}_2\text{S}_3$  when a voltage  
70 is applied through Ag electrodes. We studied this effect on the crystallisation  
process as a function of electric field by patterning Ag electrodes, separated by  
a  $100 \mu\text{m}$ , on the surface of  $\text{Sb}_2\text{S}_3$  thin films using an e-beam evaporator and a  
shadow mask, and then applying a voltage to the Ag electrodes whilst annealing  
the sample in the microscope furnace.

75 To test the hypothesis that the electric field can influence the crystallisa-  
tion temperature, a non-isothermal crystallisation study was conducted. The  
 $\text{Sb}_2\text{S}_3$  films with Ag electrodes were heated from room temperature to 623 K at  
a rate of 2 K/min. The measurement was repeated with and without an electric  
field of 200 kV/m applied to the Ag electrodes.

80 To distinguish the influence of electric field induced Ag dissolution from that  
of thermal diffusion of Ag cations, isothermal crystallisation of  $\text{Sb}_2\text{S}_3$  thin films  
under the influence of an external electric field was also studied. The samples  
were heated at a rate of 40 K/min to 493 K, equilibrated for 1 minute, and  
then heated at 10 K/min to the measurement temperature of 513 K. At this  
85 temperature, the crystallisation was studied as a function of electric field.

We have now shown that the crystallisation temperature of  $\text{Sb}_2\text{S}_3$  is lowered  
by Ag doping, and electric field can be used to dope Ag into  $\text{Sb}_2\text{S}_3$  from the  
Ag electrodes. When an electric field is applied to Ag electrodes at high tem-  
perature, both a thermal effect and an electric field induced Ag doping effect

90 will influence the crystallisation temperature. To show this, we conducted an isothermal crystallisation study of  $\text{Sb}_2\text{S}_3$  with and without Ag electrodes. The measurements were performed at temperatures ranging from 528 K to 548 K at 5 K intervals.

We analysed the crystallisation process of the  $\text{Sb}_2\text{S}_3$  using microphotography. Images were collected through a  $10\times$  objective lens at a rate of one picture per second. We found that the optical contrast between the crystalline and amorphous regions was greatest when we used "red-blue" colour channels. The "UU" image analysis tool[25] was used to determine the amorphous and crystalline areas of the film by setting an intensity threshold that was defined as  $\frac{(R-B)_{cryst}+(R-B)_{amor}}{2}$ . Values below the threshold were considered to be amorphous whilst values above the threshold were considered to be crystalline.

The crystallisation incubation time was estimated using the generalised Johnson-Mehl-Avrami-Kolmogorov (JMAK) equation[26]:

$$x(t) = 100 - 100e^{-\frac{CI(t)U^m t^{m+1}}{m+1}} \quad (1)$$

$$105 \quad I(t) = I^{ss} * \left(\frac{4\pi\tau}{t}\right)^{1/2} e^{-\frac{\pi^2\tau}{4t}} \quad (2)$$

where  $x(t)$  is crystallinity as a function of time,  $C$  is the geometric factor,  $m$  is dimensionality factor,  $I(t)$  is the crystal nucleation rate,  $U$  is the crystal growth rate,  $\tau$  is the incubation time, and  $I^{ss}$  is the steady-state rate of nucleation of crystalline clusters.

110 The microscope images of the samples that were crystallised in an electric field showed filaments forming from the Ag cathode toward the anode. To establish the origin of these filaments, we performed X-ray fluorescence mapping at beam line 37XU of SPring-8, Japan. Micro-focusing optics with a nominal spot size of 100 nm were used in the scanning X-ray microprobe system. Samples of  $\text{Sb}_2\text{S}_3$  with silver electrodes were mounted on an X-Y stage. The energy dispersive detector, which was used to measure the fluorescence signal from the sample, was placed perpendicular to the incident X-ray beam to minimise elastic scattering contributions from the sample's substrate.

Density functional theory molecular dynamics (DFT-MD) modelling was performed using the Vienna Ab-initio Simulation Package (VASP)[27], version

5.3.2, with PAW-pseudopotentials[28], PBEsol exchange-correlation functional[29], 3 fs timestep, periodic boundary conditions (PBC), and an NVT ensemble with a Nosé thermostat[30, 31, 32]. For quenching the molten model with a negative temperature ramp, a velocity rescaling algorithm was used. Energies were  
125 calculated at the  $\Gamma$ -point of the Brillouin zone ( $\mathbf{k}=0$ ).

A randomly generated structure with 60 S, 40 Sb, and 1 Ag atom was optimised by a conjugate gradient algorithm. The optimised structure was cooled from 3000 K to 1500 K in a 50 ps simulation and equilibrated at 1500 K for 20 ps to obtain a model for liquid Ag-Sb<sub>2</sub>S<sub>3</sub> with 1% Ag content.

130 The self-diffusion constant  $D^*$  can be calculated from MD simulation trajectory as  $D^* = \frac{1}{N} \sum_{i=1}^N \frac{(\Delta \vec{r}_i)^2}{6\Delta t}$ , where  $\vec{r}_i$  are the positions of the atoms 1-N, and  $t$  is the time in simulation. To study diffusion at 300-1000 K, the liquid Ag-Sb<sub>2</sub>S<sub>3</sub> structure was equilibrated at each temperature, and three 15 ps simulations per temperature were performed. The diffusion constant was calculated  
135 for each run over the 15 ps trajectory, and then averaged over the three runs for each temperature. The pair distribution functions were calculated from a sample of one structure every 0.03 ps (500 structures for a 15 ps trajectory) in the three diffusion runs.

We analysed the relationship between cavities in the amorphous structure  
140 and atomic species using the pyMolDyn[33] software with  $270 \times 270 \times 270$  point domain grid (0.05 Å grid spacing) and 2.6 Å atom radius. The cavity center point was defined as the center of the largest sphere that can be placed inside the cavity.

## RESULTS AND DISCUSSION

145 Ag doping significantly lowers the crystallisation temperature of Sb<sub>2</sub>S<sub>3</sub> from 585 K for undoped Sb<sub>2</sub>S<sub>3</sub> to 488 K with 12 at.% Ag doping. Figure 1 shows the crystallisation temperature of the Ag-doped Sb<sub>2</sub>S<sub>3</sub> films as a function of Ag content. The 2 K error bars originate from random errors associated with starting the data collection. Higher doping concentrations result in an apparent

150 reduction in crystallisation temperature. We note that there appears to be two  
 physical mechanisms that influence the crystallisation temperature at different  
 silver doping concentrations. We have fitted an exponential curve to doping  
 concentrations lower than 4 at.% and a linear curve to the higher doping con-  
 centrations, as shown in figure 1. These fits are purely to guide the readers' eye  
 155 and we refrain from interpreting the physical meaning of the fitting constants.  
 However, the results clearly show that the  $\text{Sb}_2\text{S}_3$  crystallisation temperature  
 depends on Ag doping. It is worth noting that phase separation is observed  
 in the as-deposited  $\text{Sb}_2\text{S}_3$  thin films when the silver concentration is higher  
 than 8 at.%. For lower Ag concentrations, phase separation is not observed  
 160 and the as-deposited thin film appears uniform. For Ag concentrations greater  
 than 8 at.%, Ag nanoparticles are formed on the surface of the as-deposited  
 $\text{Sb}_2\text{S}_3$  film, the SEM images of 4 at.% and 8 at.% Ag doped  $\text{Sb}_2\text{S}_3$  are shown  
 in insets in figure 1. This agrees with other reports that show a limit to the  
 concentration of Ag dissolved into chalcogenides. For example, the limit for Ag  
 165 doping into  $\text{Sb}_{33}\text{S}_{67}$  is  $\sim 10$  at.% [23, p. 169].

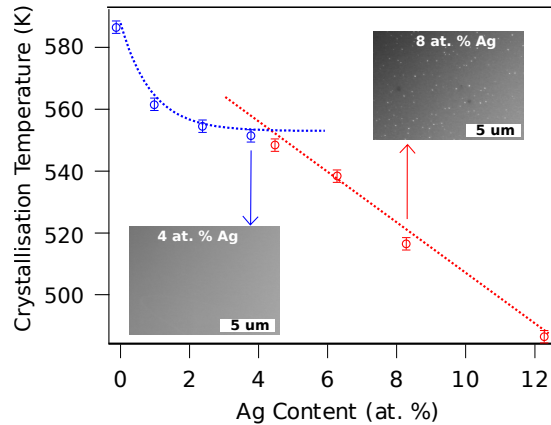


Figure 1: Ag doped  $\text{Sb}_2\text{S}_3$  crystallisation temperature. Inset: SEM images of sample surface for 4 at.% and 8 at.% Ag doping.

A non-isothermal crystallisation study of  $\text{Sb}_2\text{S}_3$  with Ag electrodes was conducted to test the hypothesis that the electric field can influence the crystalli-



sation temperature. Figure 2 shows that crystallisation begins at 557 K when there is no electric field applied to the film. However, when 200 kV/m electric field is applied, the crystallisation temperature is lowered by 22 K to 535 K. The effect of electric field on the peak crystallisation rate is compared in figure 2(b). At 535 K, the crystallisation rate with 200 kV/m electric field is 3.8 %/s, which is substantially higher than 0.043 %/s, which we measured without the electric field at the same temperature. The crystallisation temperature is lowered by the electric field, although the peak crystal growth rate is higher when no electric field is applied. This is interesting because it implies that electric field affects the nucleation rate but not the crystal growth rate. Figure 2 indicates that with the driving force of the electric field, the Ag atoms tend to disolute and then diffuse from one electrode to the other, substantially decreasing the crystallisation temperature. Thus we conclude that the applied electric field strongly influences the crystallisation kinetics. Furthermore, crystallisation proceeds from the cathode, which implies that the Ag cations are responsible for the electric field dependent crystallisation effect.

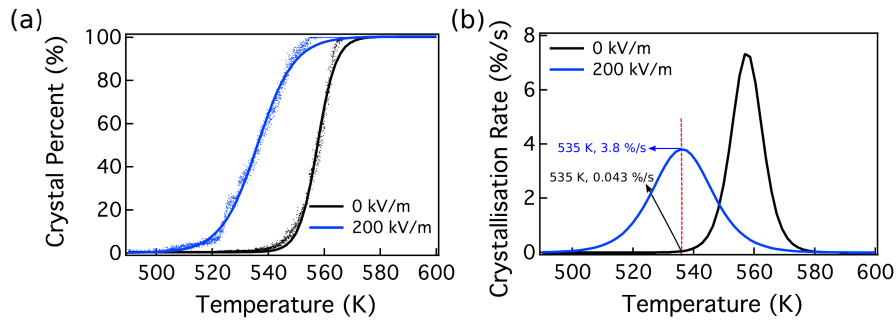


Figure 2: (a) Crystal percentage as a function of temperature with 0 kV/m (black) and 200 kV/m (blue) applied to the  $\text{Sb}_2\text{S}_3$  film through Ag electrodes. (b) The crystal growth rate as a function of temperature with 0 kV/m (black) and 200 kV/m (blue) applied.

To measure the influence of the electric field on nucleation, an isothermal crystallisation study of  $\text{Sb}_2\text{S}_3$  with and without Ag electrodes was conducted. As shown in figures 3 (a) and (c), the crystallisation rate is relatively low at 528 K, and the crystallinity is around 30 % after 8060 seconds. The crystallisation

rate is accelerated by elevating the annealing temperature to 548 K, where the film is completely crystallised after 1500 seconds. The peak crystal growth rate increases from 0.013 %/s at 528 K to 0.16 %/s at 548 K.

The electric field promotes silver dissolution into the  $\text{Sb}_2\text{S}_3$  film, and it significantly increases the crystallisation rate. Figures 3(b) and (d) show the influence of the electric field on the crystallisation rate of  $\text{Sb}_2\text{S}_3$  at a constant temperature of 513 K. Increasing the applied electric field from 50 kV/m to 200 kV/m reduces the time for complete crystallisation by 79%, from 6200 seconds to 1300 seconds. To achieve a similar crystallisation rate with no electric field it would be necessary to increase the annealing temperature to 548 K. The peak crystal growth rate increases from 0.1 %/s at 50 kV/m to 0.36 %/s at 200 kV/m, which is more than an order of magnitude higher than that of a sample without an applied electric field at 528 K. By fitting the generalised Johnson-Mehl-Avrami-Kolmogorov (JMAK) equation[26] to the crystallinity versus time plots in figure 3(b), the effect of the electric field induced Ag doping on the crystal nuclei incubation time was estimated, as shown in the inset of figure 3(d). The length of the incubation time reflects the difficulty to initiate crystallisation. Stable crystal nuclei are required for the onset of crystal growth. As the electric field is increased, the crystallisation rate increases and the incubation time decreases, as shown in inset of figure 3(d). The incubation time is reduced by 75 % when the applied electric field is increased from 50 kV/m to 200 kV/m. Furthermore, comparing 528 K and 0 V/m in figure 3(c) with an electric field of 200 kV/m at an even lower temperature of 513 K in figure 3(d), we see the crystallisation rate increases from 0.013 %/s to 0.36 %/s.

Increasing the annealing temperature or applying an electric field to the two silver electrodes accelerates the crystallisation rate. Higher temperatures provide more energy to overcome interfacial energy difference between the amorphous and crystalline phases thus result in facilitated crystal growth. Whereas the electric field increases silver content in  $\text{Sb}_2\text{S}_3$ , which creates voids in the amorphous structure. The voids accelerate the nucleation process and consequently reduce the time needed for full crystallisation. The proposed model to

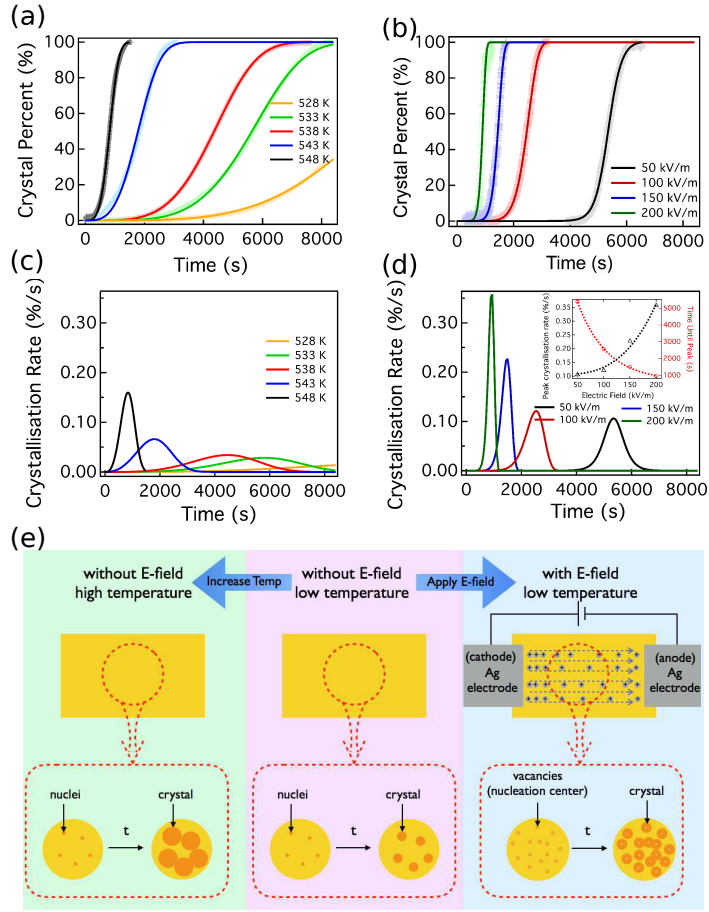


Figure 3: Isothermal crystallisation dependence on temperature and electric field. (a) Crystallinity as a function of time for pure  $\text{Sb}_2\text{S}_3$  films measured at different temperatures and the associated growth rate (c). For a sample held under isothermal conditions at 513 K, the effect of electric field on the crystallinity is shown in (b) and the associated growth rates are given in (d). The inset in (d) shows the crystal nuclei incubation time and the crystal growth rate as a function of electric field intensity. A model proposed to explain the electric field effect and temperature effect is given in (e). The white dots indicate the voids caused by diffusion of silver.

220 explain the influence of increasing temperature and applying an electric field is illustrated in figure 3(e).

The silver distribution in the  $\text{Sb}_2\text{S}_3$  film between the electrodes provides evidence in support of electric field induced silver drift in  $\text{Sb}_2\text{S}_3$ . We compared

X-ray fluorescence (XRF) elemental maps for samples crystallised with and without an electric field of 150 kV/m at room temperature and 513 K, see figure 4. With the increased temperature and electric field, a silver filament can be observed between the electrodes, see figure 4(b). The electric field appears to enhance the drift of silver, and the effect is further enhanced at elevated temperatures.

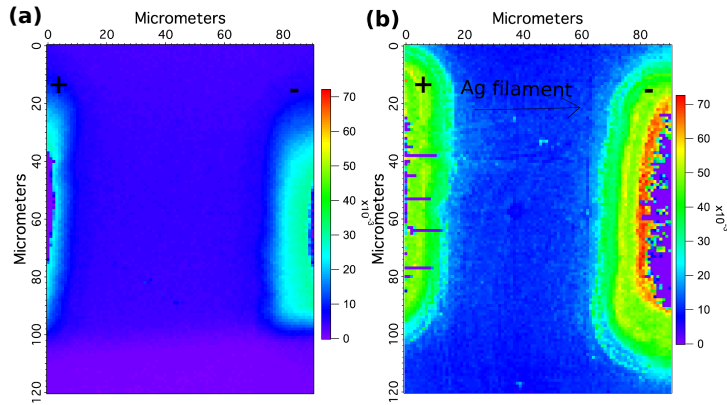


Figure 4: Fluorescence mapping of silver on  $\text{Sb}_2\text{S}_3$  with Ag electrodes under different temperature and electric field. Silver electrodes separation is around  $75 \mu\text{m}$ , and scan area is  $90 \mu\text{m}$  by  $120 \mu\text{m}$ . (a) room temperature, 0 kV/m; (b) 513 K, 150 kV/m, after 30 minutes.

The movement of Ag, Sb and S atoms at elevated temperatures was studied computationally with density functional theory molecular dynamics (DFT-MD) simulations. The diffusion coefficients of the three elements at different temperatures were obtained from the model, and are shown in figure 5(a). The diffusion constant of Ag is significantly higher than that of Sb or S, this indicates that the Ag ions are mobile in the solid amorphous  $\text{Sb}_2\text{S}_3$  film. The optimum temperature to diffuse Ag into  $\text{Sb}_2\text{S}_3$  is between 400 K and 500 K. The reason for this can be found from the cavity (or void) distribution around atoms of different elements. As shown in figure 5(b), at 300 K cavities are more common around Sb and S atoms than Ag atoms at  $\sim 2.7 \text{ \AA}$ , which is close to a typical bond length in  $\text{Sb}_2\text{S}_3$ . This can hinder Ag diffusivity as there is insufficient room around the

240 Ag atoms. However, there is a significant number of cavities around Ag atoms  
 at slightly longer distances close to 3.0 Å, and when the temperature is increased  
 to 400 K, these cavities move closer to Ag atoms; the average Ag-cavity distance  
 is shorter than S-cavity and Sb-cavity. This gives Ag atoms sufficient room to  
 move, and increases their diffusivity in comparison to Sb and S atoms. It shows  
 245 that in 600 K the cavity concentration around Ag atoms is less than around Sb  
 or S atoms, giving further weight to the explanation, as the Ag diffusion in 600  
 K is lower in comparison to 500 K while Sb and S diffusivities are increasing  
 (probably due to thermal contribution).

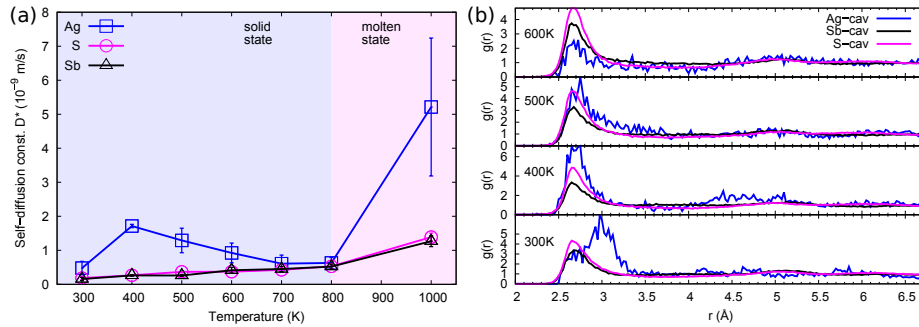


Figure 5: Self-diffusion constant of Ag, S and Sb atoms as a function of temperature (a). Partial pair distribution functions of cavities for Ag, Sb and S atoms in DFT-MD simulations (b).

In conclusion, Ag doping substantially reduces the crystallisation tempera-  
 250 ture of  $\text{Sb}_2\text{S}_3$ . The  $\text{Sb}_2\text{S}_3$  crystallisation temperature, crystallisation rate and  
 direction, and the crystal nuclei can be enhanced by applying an electric field  
 to  $\text{Sb}_2\text{S}_3$  through Ag electrodes. The crystal nuclei incubation time decreases  
 substantially when 200 kV/m is applied to the film through the Ag electrodes.  
 X-ray fluorescence mapping shows clear Ag filament formed when an electric  
 255 field is applied at elevated temperatures. The DFT-MD modelling results show  
 that the Ag atoms are mobile in amorphous  $\text{Sb}_2\text{S}_3$  and the optimum tempera-  
 ture to diffuse Ag into  $\text{Sb}_2\text{S}_3$  is between 400 K and 500 K, due to Ag atoms  
 locating at cavities within the amorphous network. This is in agreement with  
 the experimental results. We believe that this electric field enhanced crystalli-

260 sation property could have application in non-Von Neuman logic, where the materials' electrical response is non-linear with voltage[34].

## Acknowledgement

This work was supported by the SUTD International Design Center under the grant IDSF1200108OH and the Singapore Agency for Science, Technology  
265 and Research (A\* STAR) funded Singapore-China joint research program under the grant 1420200046. We are grateful for beam time on BL37XU at SPring-8 (proposal 2014A1170) and the technical support of Dr Yasuko Terada. JK is grateful for his SUTD-MIT postdoctoral fellowship. CS acknowledges support from the A\*star (1223600007) and the Singapore Ministry of Education  
270 (MOE2011-T3-1-005). MK acknowledges support from Center of Materials and Nanotechnologies, Czech Rep, European Fund CZ.1.05/4.1.00/11.0251.

## References

- [1] J. Varghese, S. Barth, L. Keeney, R. W. Whatmore, J. D. Holmes, Nanoscale ferroelectric and piezoelectric properties of sb2s3 nanowire arrays, *Nano lett.* 12 (2) (2012) 868–872.
- [2] J. Chao, B. Liang, X. Hou, Z. Liu, Z. Xie, B. Liu, W. Song, G. Chen, D. Chen, G. Shen, Selective synthesis of Sb2S3 nanoneedles and nanoflowers for high performance rigid and flexible photodetectors, *Opt. Express* 21 (11) (2013) 13639–13647.
- [3] P. Pustková, Z. Zmrhalová, J. Málek, The particle size influence on crystallization kinetics of (GeS2)0.1(Sb2S3)0.9 glass, *Thermochim. Acta* 466 (1) (2007) 13–21.
- [4] V. Rinkevichius, M. Mikalkevichius, Pyroelectric effect in antimony trisulfide single crystals, *Sov. Phys. Solid State USSR* 9 (10) (1967) 2360.
- [5] O. Savadogo, K. C. Mandal, Studies on new chemically deposited photoconducting antimony trisulphide thin films, *Sol. Energ. Mat. Sol. C.* 26 (1) (1992) 117–136.
- [6] S. Messina, M. Nair, P. Nair, Solar cells with Sb2S3 absorber films, *Thin Solid Films* 517 (7) (2009) 2503–2507.
- [7] X. Zhou, L. Bai, J. Yan, S. He, Z. Lei, Solvothermal synthesis of Sb2S3/C composite nanorods with excellent li-storage performance, *Electrochim. Acta* 108 (2013) 17–21.
- [8] J. Ma, X. Duan, J. Lian, T. Kim, P. Peng, X. Liu, Z. Liu, H. Li, W. Zheng, Sb2S3 with various nanostructures: controllable synthesis, formation mechanism, and electrochemical performance toward lithium storage, *Chem-Eur. J.* 16 (44) (2010) 13210–13217.
- [9] P. V. Prikhodchenko, J. Gun, S. Sladkevich, A. A. Mikhaylov, O. Lev, Y. Y. Tay, S. K. Batabyal, D. Y. Yu, Conversion of hydroperoxoantimonate



- coated graphenes to Sb<sub>2</sub>S<sub>3</sub>@ graphene for a superior lithium battery anode,  
300 Chem. Mater. 24 (24) (2012) 4750–4757.
- [10] C. Yan, G. Chen, R. Jin, X. Zou, H. Xu, C. Lv, Well-defined Sb<sub>2</sub>S<sub>3</sub> nanostructures: citric acid-assisted synthesis, electrochemical hydrogen storage properties, Cryst. Res. Technol. 48 (8) (2013) 566–573.
- [11] F. Cao, W. Liu, L. Zhou, R. Deng, S. Song, S. Wang, S. Su, H. Zhang,  
305 Well-defined Sb<sub>2</sub>S<sub>3</sub> microspheres: High-yield synthesis, characterization, their optical and electrochemical hydrogen storage properties, Solid State Sciences 13 (6) (2011) 1226–1231.
- [12] H. Zhang, M. Ge, L. Yang, Z. Zhou, W. Chen, Q. Li, L. Liu, Synthesis and catalytic properties of Sb<sub>2</sub>S<sub>3</sub> nanowire bundles as counter electrodes for  
310 dye-sensitized solar cells, J. Phys. Chem. C 117 (20) (2013) 10285–10290.
- [13] S. Shaji, A. Arato, J. O’Brien, J. Liu, G. A. Castillo, M. M. Palma, T. D. Roy, B. Krishnan, Chemically deposited Sb<sub>2</sub>S<sub>3</sub> thin films for optical recording, J. Phys. D: Appl. Phys. 43 (7) (2010) 075404.
- [14] T. Wagner, G. Dale, P. Ewen, A. Owen, V. Perina, Kinetics of the thermally  
315 and photoinduced solid state reaction of Ag with as<sub>33</sub>s<sub>67</sub> films, J. Appl. Phys. 87 (11) (2000) 7758–7767.
- [15] T. Wagner, Photo-and thermally-induced diffusion and dissolution of Ag in chalcogenide glasses thin films, J. Optoelectron. Adv. M. 4 (3) (2002) 717–727.
- 320 [16] T. Wagner, S. Kasap, M. Vlček, M. Frumar, P. Nesladek, M. Vlček, The preparation of the Ag<sub>x</sub>(As<sub>0.33</sub>S<sub>0.67</sub>)<sub>100-x</sub> amorphous films by optically-induced solid state reaction and the films properties, Appl. Surf. Sci. 175 (2001) 117–122.
- [17] T. Wágner, J. Gutwirth, M. Krbal, M. Vlček, M. Vlček, M. Frumar, Ag-Sb-S  
325 amorphous chalcogenide thin films prepared by optically induced dissolution and diffusion of silver, J. Non-Cryst. Solids 326 (2003) 238–242.

- [18] M. Vl, Physical properties and structure of amorphous Agx (Sb<sub>0.33</sub>S<sub>0.67</sub>)<sub>100-x</sub> prepared by optically-induced diffusion and dissolution of silver into spin-coated amorphous Sb<sub>33</sub>S<sub>67</sub> films and their application for optical recording, *J. Optoelectron. Adv. M.* 5 (5) (2003) 1139–1146.
- [19] T. Kosa, R. Rangel-Rojo, E. Hajto, P. Ewen, A. Owen, A. Kar, B. Wherrett, Nonlinear optical properties of silver-doped As<sub>2</sub>S<sub>3</sub>, *J. Non-Cryst. Solids* 164 (1993) 1219–1222.
- [20] C. Huang, D. Hewak, Silver-doped germanium sulphide glass channel waveguides fabricated by chemical vapour deposition and photo-dissolution process, *Thin Solid Films* 500 (1) (2006) 247–251.
- [21] K. J. Koski, C. D. Wessells, B. W. Reed, J. J. Cha, D. Kong, Y. Cui, Chemical intercalation of zerovalent metals into 2d layered Bi<sub>2</sub>Se<sub>3</sub> nanoribbons, *J. Am. Chem. Soc.* 134 (33) (2012) 13773–13779.
- [22] M. Mitkova, Y. Sakaguchi, D. Tenne, S. K. Bhagat, T. L. Alford, Structural details of ge-rich and silver-doped chalcogenide glasses for nanoionic nonvolatile memory, *Phys. Status Solidi A* 207 (3) (2010) 621–626.
- [23] A. V. Kolobov, Photo-induced metastability in amorphous semiconductors, John Wiley & Sons, 2006.
- [24] Y. Sato, H. Akizuki, T. Kamiyama, Y. Shigesato, Transparent conductive nb-doped TiO<sub>2</sub> films deposited by direct-current magnetron sputtering using a TiO<sub>2-x</sub> target, *Thin Solid Films* 516 (17) (2008) 5758–5762.
- [25] L. Chen, An image-processing software package: Uu and fig for optical metrology applications, in: International Conference on Optics in Precision Engineering and Nanotechnology (icOPEN2013), International Society for Optics and Photonics, 2013, pp. 87690U–87690U.
- [26] S. Senkader, C. Wright, Models for phase-change of Ge<sub>2</sub>Sb<sub>2</sub>Te<sub>5</sub> in optical and electrical memory devices, *J. Appl. Phys.* 95 (2) (2004) 504–511.

- 355 [27] G. Kresse, J. Hafner, Ab initio molecular dynamics for open-shell transition metals, *Phys. Rev. B* 48 (17) (1993) 13115.
- [28] G. Kresse, D. Joubert, From ultrasoft pseudopotentials to the projector augmented-wave method, *Phys. Rev. B* 59 (3) (1999) 1758.
- [29] J. P. Perdew, A. Ruzsinszky, G. I. Csonka, O. A. Vydrov, G. E. Scuse-  
360 ria, L. A. Constantin, X. Zhou, K. Burke, Restoring the density-gradient expansion for exchange in solids and surfaces, *Phys. Rev. Lett.* 100 (13) (2008) 136406.
- [30] S. Nosé, A unified formulation of the constant temperature molecular dynamics methods, *J. Chem. Phys.* 81 (1) (1984) 511–519.
- 365 [31] N. Shuichi, Constant temperature molecular dynamics methods, *Prog. Theor. Phys. Supp.* 103 (1991) 1–46.
- [32] D. Bylander, L. Kleinman, Energy fluctuations induced by the nosé thermostat, *Phys. Rev. B* 46 (21) (1992) 13756.
- [33] J. Kalikka, J. Akola, R. Jones, Simulation of crystallization in Ge<sub>2</sub>Sb<sub>2</sub>Te<sub>5</sub>:  
370 A memory effect in the canonical phase-change material, *Phys. Rev. B* 90 (18) (2014) 184109.
- [34] T. Ohno, T. Hasegawa, T. Tsuruoka, K. Terabe, J. K. Gimzewski, M. Aono, Short-term plasticity and long-term potentiation mimicked in single inorganic synapses, *Nat. Mater.* 10 (8) (2011) 591–595.